Aspects of seismic imaging using P-SV converted waves

David W.S. Eaton and Robert R. Stewart

ABSTRACT

Several aspects of processing P-SV data are more complex than the conventional P-wave processing case. In this study, four processes that pertain directly to the seismic imaging problem are examined: S1-S2 wave field separation, P-SV common conversion point (CCP) mapping, moveout correction and time migration. If a low-velocity near surface layer is present, fast and slow (split) shear waves recorded at the free surface can be separated prior to stack using a simple co-ordinate rotation. Current methods of CCP gathering for multifold P-SV data may result in excessive loss of spatial resolution. A new method is proposed to solve this problem by mapping each data sample to its correct conversion point position before stacking. Examples of this technique are provided using synthetic data. The coefficients of the power series expansion for the squared traveltime for P-SV reflections are similar to the coefficients for the equivalent power series in the P-P case, and suggest that P-SV moveout is nearly hyperbolic. However, the hyperbolic moveout approximation is less accurate for P-SV events than P-P events. Finally, conventional time migration appears to produce valid results when applied to P-SV data after stack.

INTRODUCTION

Why record P-SV converted reflections?

Historically, seismic reflection data have been acquired and processed to enhance primary reflected P waves in the final section, although both P waves and S waves are generated within the earth. An alternative image of the same part of the subsurface can be obtained using S waves, in much the same way as the conventional P-wave image. Interest in interpreting concurrent P-wave and S-wave images of the same part of the subsurface has developed recently for several reasons:

- to provide an independent estimate of geological structure to complement the interpretation of P-wave data;
- to provide an accurate tool for the measurement of Poisson's ratio, which may give clues regarding rock lithology (Tatham, 1982);
- to calibrate P-wave bright spots (Ensley, 1984; Robertson and Pritchett, 1985);
- to identify and characterize vertical fracture systems by the analysis of shear wave birefringence (Crampin, 1985).

The most common method for acquiring S-wave data on land is by direct generation of SH-waves using seismic sources adapted for this purpose (McCormack and Tatham, 1986). However, the near surface weathered layer is often a strongly attenuating medium for shear waves, and may also contribute to very large, short wavelength shear wave statics (McCormack and Tatham, 1986). This problem may also be more acute in Western Canada than other regions due to the ubiquitous covering of Pleistocene glacial till. It can therefore be advantageous to utilize mode-converted SV waves and thereby reduce the shear wave path length

within the weathered by one half. This study will be concerned only with the case of mode-converted shear waves (ie. P-SV), rather than SH-SH reflections.

Processing Considerations

The underlying theory for the process of obtaining a migrated zero offset seismic image using multifold P-P surface data is well understood (eg. Yilmaz, 1987). However, certain differences between the propagation of P waves and S waves within an elastic medium renders the P-SV imaging process less straightforward than the P-P case. In this study, four aspects relevant to processing of P-SV converted wave data are considered:

- wave field separation of split shear waves;
- depth variant CCP mapping;
- non-hyperbolic moveout correction;
- post-stack time migration.

All four of these processes are fundamental to obtaining a correct subsurface image using P-SV converted waves. Furthermore, application of any of these requires modification to existing algorithms designed for P-P waves, or implementation of new algorithms.

The phenomenon of birefringence, exhibited in a medium characterized by azimuthal anisotropy, is unique to shear waves. When birefringence occurs, shear waves split into two modes of propagation having slightly different velocities and particle motion that are nearly mutually orthogonal (Crampin, 1981). The directions of particle motion for the polarized shear waves establishes a natural co-ordinate system in the horizontal plane. Unless horizontal measurements are confined to the natural co-ordinate axes, the two shear wave arrivals will interfere, potentially resulting in poor signal quality and line misties. In addition, certain studies (eg Willis *et al.*, 1986) suggest that azimuthal anisotropy in sedimentary basins may be widespread. Hence, some method of separating split shear waves is a requirement in general. Previous studies (Alford, 1986; Thomsen, 1988) have outlined techniques for rotation of the horizontal data components into the natural co-ordinate system after stack. However, the post-stack approach has certain shortcomings, because the stacking velocities of split shear wave modes differ (Thomsen, 1988) and interference between the two modes may degrade data dependent processing steps (eg. automatic residual statics). Therefore, it would be advantageous to separate split shear waves prior to stacking.

Another significant difference between processing of multifold converted wave data and conventional P-wave data is the method used to perform CCP sorting. The position of the conversion point for a single layer is a function of depth, offset and the Poisson's ratio (σ) of the layer (Tessmer and Behle, 1988; Taylor, 1989). Commonly used methods for gathering traces at an approximate conversion point result in excessive loss of spatial resolution for shallower reflectors (Slotboom and Stewart, 1989). Several alternative approaches are to selectively gather traces for specific target depths using Tessmer and Behle's (1988) conversion point formula, or to relocate each sample to its true conversion point location prior to stack. Moveout correction of long offset converted data is also complicated because the hyperbolic moveout approximation normally applied to conventional data is not as accurate for converted waves (Tessmer and Behle, 1988). Superior results can be obtained using a higher order approximation to the traveltime formula.

Finally, the accuracy and limitations of time migration of P-SV converted wave data require careful scrutiny. Time migration of conventional P-wave data uses *acoustic* wave theory applicable to data recorded with zero offset and is based on the assumption that lateral velocity variations are mild (Yilmaz, 1987, p. 242). Although acoustic theory is not strictly valid even for P-P reflections, experience

has demonstrated that conventional migration can nevertheless yield adequate results. It has not been established, however, if the same migration principles can be extended further to apply to stacked P-SV converted wave data.

Objectives, assumptions and limitations

The goal of this study is to refine and establish techniques for the construction of migrated seismic images of the subsurface from stacked data using P-SV reflections that can be compared directly to a migrated P-P seismic section. The methods used are dictated by both theoretical validity and computational efficiency. While it is possible to achieve the goal of seismic imaging by application of inversion/migration methods based on the full elastic wave equation (eg. Mora, 1987; Beydoun and Mendes, 1989), these methods are very sensitive to the presence of noise and not presently tractable for large problems (eg. 3-D), nor to iterative application.

This study will be restricted to the case of surface sources and receivers. The earth is assumed to be only weakly anisotropic. In this way, following the separation of wave fields into P-, S1- and S2- components to compensate for the polarization effects of S-wave anisotropy, it is assumed that the earth can be treated as isotropic. In many cases the high frequency optics (ray theory) approximation is utilized, implying that the wave field in heterogeneous media encounters weak parameter contrasts and large interface radii of curvature as compared with the wavelength. In addition, horizontal velocity gradients are assumed to be small enough for the principles of time migration to be valid.

Notation

Throughout this paper, the following notation will be employed:

α	P-wave velocity
β	SV-wave velocity (isotropic case)
σ	Poisson's ratio
γ	Velocity ratio β/α
p	Ray parameter (horizontal slowness)
θ	Angle of incidence
$\mathbf{u}$	Particle velocity vector
$\tilde{v}$	rms velocity
v_m	Migration velocity
ω	Angular frequency
Δx	Source-receiver offset

WAVE FIELD SEPARATION

P-SV Separation

Wave motion at a free surface is governed by the boundary condition that components of stress in the plane of the surface must vanish. This boundary condition is almost exactly satisfied at the earth's surface; therefore the earth's surface is a very efficient reflector for seismic energy, as confirmed by the common occurrence of source "ghosts". Consequently, receivers placed at the free surface do not measure wave motion due only to an incident wave field, but the vector sum of the incident wave and the corresponding reflected and mode converted waves. The actual particle velocity components due to an incident wave having unit amplitude are (Evans, 1984; Dankbaar, 1985):

$$
\begin{aligned}
R_v^p(p) &= 2\gamma^{-1}\xi(2\beta^2p^2-1)/\psi \\
R_r^p(p) &= 4\beta p\xi\eta/\psi \\
R_v^{sv}(p) &= 4\alpha p\xi\eta/\psi \\
R_r^{sv}(p) &= 2\eta(1-2\beta^2p^2)/\psi \\
R_t^{sh}(p) &= 2 \ ,
\end{aligned}
\tag{1}
$$

where $\xi = (\gamma^2-\beta^2p^2)^{1/2}$, $\eta = (1-\beta^2p^2)^{1/2}$ and $\psi = (1-2\beta^2p^2)^2 + 4p^2\beta^2\xi\eta$, the subscript denotes the receiver orientation (vertical, radial or transverse) and the superscript denotes the type of incident wave. We can write the measured particle velocity vector at the free surface, $\mathbf{u}(x,t)$, in terms of the incident body wave vector $\mathbf{v}(x,t)$ using equations (1):

$$
\mathbf{u} = \mathbf{A}\mathbf{v} \ , \tag{2}
$$

where $\mathbf{v} = (u_p,u_{sv},u_{sh})^T$, $\mathbf{u} = (u_v,u_r,u_t)^T$ and:

$$
\mathbf{A} = \begin{bmatrix} R_v^p & R_v^{sv} & 0 \\ R_r^p & R_r^{sv} & 0 \\ 0 & 0 & 2 \end{bmatrix} \ .
$$

Because we can express the observed data in terms of the incident body wave vector in this linear fashion, it is therefore possible to separate the observed data into its incident body wave components using:

$$
\mathbf{v} = \mathbf{A}^{-1}\mathbf{u} \ , \tag{3}
$$

where

$$
\mathbf{A}^{-1} = \begin{bmatrix} C_1 & C_2 & 0 \\ C_3 & C_4 & 0 \\ 0 & 0 & 1/2 \end{bmatrix} \ ,
$$

and $C_1 = -\gamma(1-2\beta^2p^2)/2\xi$, $C_2 = \gamma^2\alpha p$, $C_3 = \beta p$ and $C_4 = (1-2\beta^2p^2)/2\eta$ (Dankbaar, 1985). Dankbaar (1985) has proposed an *f-k* filter and Chiburis et al. (1988) have proposed a τ-p filter for performing P-SV wave field separation at the free surface using (3). The method is stable (ie. $\mathbf{A}^{-1}$ is non-singular) for all $p < \beta^{-1}$. However, numerical studies have shown that in cases where a low velocity near-surface layer is present, virtually all of the incident P-wave energy is recorded by the vertical geophone and similarly virtually all of the incident SV-wave energy is recorded by the radial geophone (Eaton, 1989). For a very low velocity near-surface layer, the variable elements of $\mathbf{A}^{-1}$ approach the following values:

$$
\begin{aligned}
C_1 &\rightarrow -1/2 \qquad C_2 \rightarrow 0 \\
C_3 &\rightarrow 0 \qquad\quad C_4 \rightarrow 1/2
\end{aligned}
$$

Thus, in areas such as Western Canada where a low velocity near-surface layer is

present, the matrix $\mathbf{A}^{-1}$ becomes nearly diagonal and merely scales the data.

S1-S2 Separation

If shear wave birefringence has occurred somewhere along the raypath of a reflected SV wave, then the polarization of the first arrival (S1) is determined by the symmetry of the last anisotropic layer through which it passed (Crampin, 1985), where the polarization angle ε is given by $\tan^{-1}(u_{sh}/u_{sv})$ (Nuttli and Whitmore, 1962). The delayed shear arrival will have polarization angle $\approx \varepsilon+\pi/2$. Equation (2) can thus be rewritten:

$$\mathbf{u} = \mathbf{B}\mathbf{v}', \tag{4}$$

where $\mathbf{v}' = (u_p, u_{s1}, u_{s2})^T$, and:

$$\mathbf{B} = \begin{bmatrix} R_v^p & \cos\varepsilon R_v^{sv} & -\sin\varepsilon \\ R_r^p & \cos\varepsilon R_r^{sv} & -\sin\varepsilon \\ 0 & 2\sin\varepsilon & 2\cos\varepsilon \end{bmatrix} .$$

It can be verified that $\mathbf{B}^{-1}$ is factorable into:

$$\mathbf{B}^{-1} = \mathbf{A}^{-1}\mathbf{R} , \tag{5}$$

where $\mathbf{R}$ represents a counterclockwise rotation through ε:

$$\mathbf{R} = \begin{bmatrix} 1 & 0 & 0 \\ 0 & \cos\varepsilon & \sin\varepsilon \\ 0 & -\sin\varepsilon & \cos\varepsilon \end{bmatrix} .$$

As discussed in the previous section, if a low velocity near-surface layer is present the matrix $\mathbf{A}^{-1}$ becomes nearly diagonal and P-SV separation is not necessary. In this situation, S1-S2 separation can be performed by a simple co-ordinate rotation. In previously published studies involving S1-S2 separation, co-ordinate rotation is performed after stacking (eg. Thomsen, 1988; Garotta and Granger, 1988). However, it is preferable to perform this separation prior to stack in order to obtain the correct stacking velocities and to improve the performance of data dependent processing operations, such as automatic residual statics.

Figure 1 shows an example in which S1-S2 wave field separation has been applied to a ray-traced multicomponent shot record. The synthetic shot records were generated using sonic log data from a Cardium oil well located at 16-1-53-13 W5, assuming a velocity ratio γ of 0.526 for shales and 0.588 for sands, and a pervasive shear wave anisotropy of 2% oriented 30° clockwise to the survey co-ordinate system. No low velocity near-surface layer was employed in the ray tracing, so P-wave artifacts are visible on the radial component record (Figure 1a). The full wave field separation has removed the P-wave artifacts and has eliminated the interference between the fast and slow shear arrivals. Note for example that the Cardium zone (CZ) appears as three distinct peaks on the radial and transverse records, but is resolved into only two peaks on the separated records.

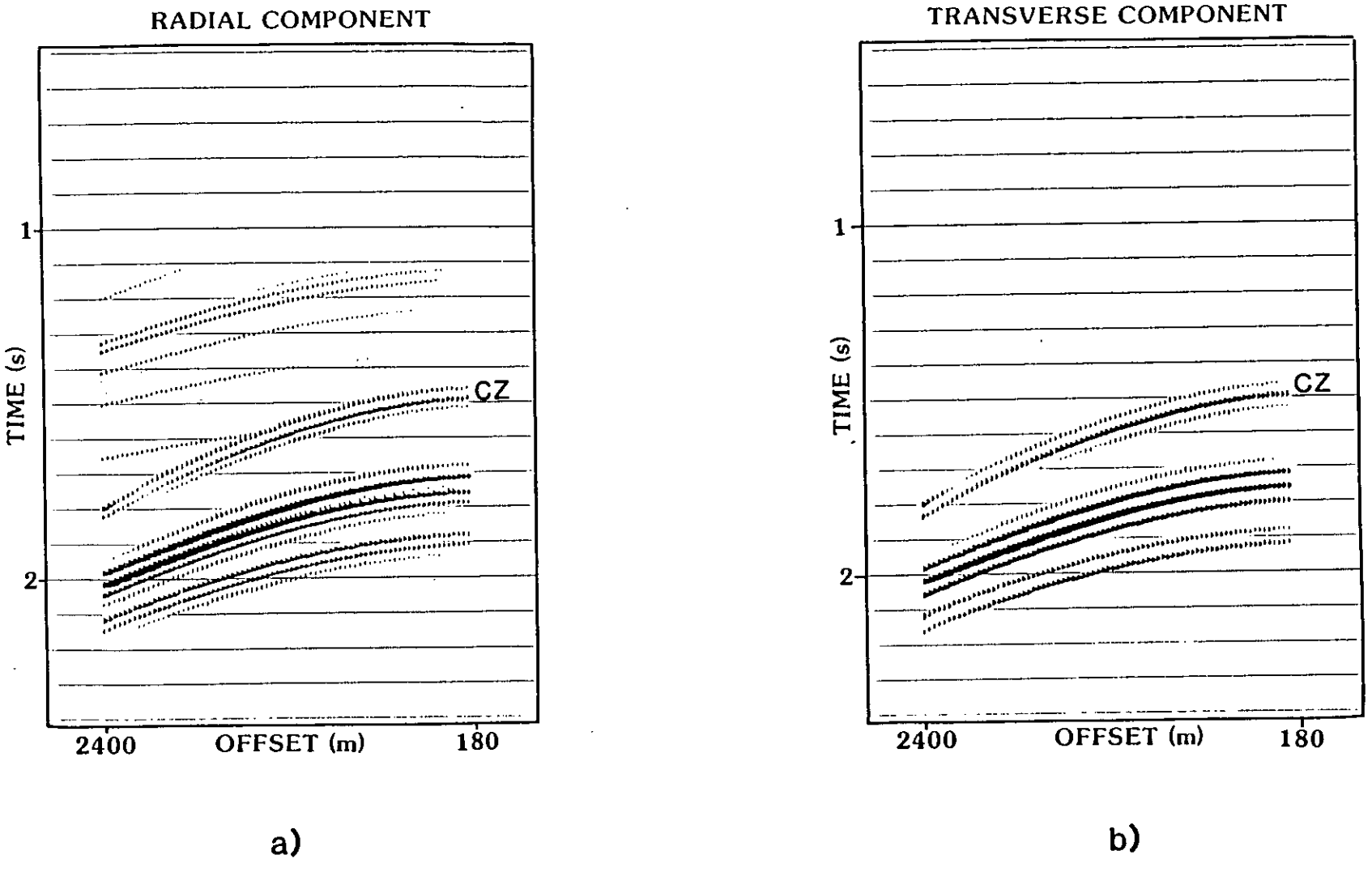

FIG. 1. (a) Radial component of synthetic shot record for 16-1-53-13 W5 with an assumed pervasive 2% azimuthal anisotropy oriented 30° clockwise with respect to the survey co-ordinate system. Note P-wave artifacts. The Cardium Zone (CZ) appears as three distinct peaks. (b) Transverse component of synthetic shot record.

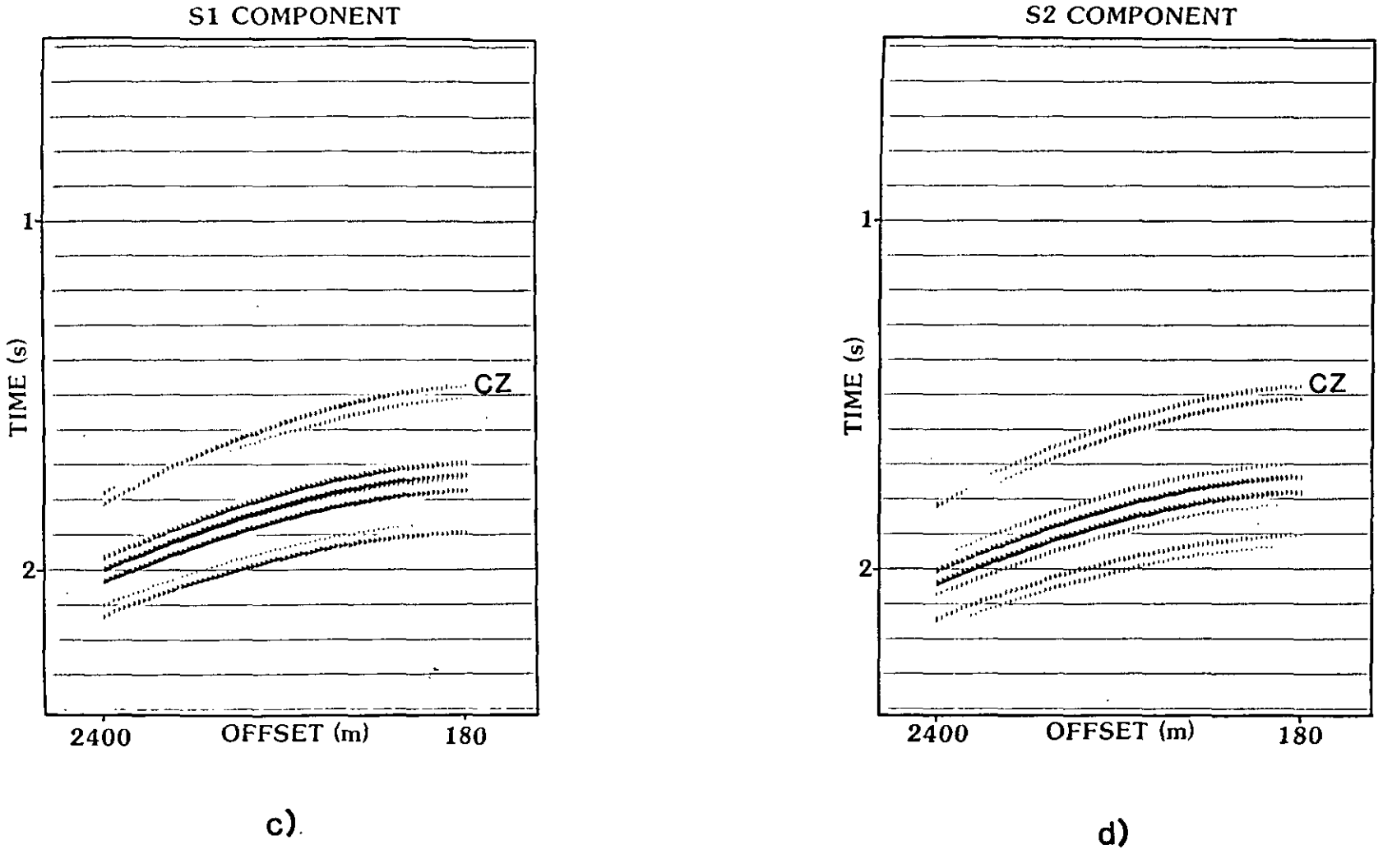

FIG. 1. (c) Separated S1 (fast) component of synthetic shot record. (d) Separated S2 (slow) component of synthetic shot record. Note that following wave field separation the Cardium Zone (CZ) appears as two peaks rather than three.

P-SV CCP MAP

Theory

Two physical aspects of P-SV wave propagation render the problem of prestack sorting of traces more difficult than is the case for P-P reflections:

- the position of the P-SV mode conversion point does not occur at the source-receiver midpoint, even for a simple layered earth;
- the position of the conversion point varies with depth in general.

To illustrate the first point, consider the raypath geometry for a P-SV converted wave event (Figure 2a). The position of the mode conversion point, x_p, is offset away from the source-receiver midpoint toward the receiver, as a direct consequence of Snell's Law; hence traces having a common midpoint do not share a CCP. It is therefore necessary to determine some other method of sorting traces prior to stacking.

Now consider a series of horizontal layers (Figure 2b). The position of the mode conversion point at each interface varies with depth. The conversion point is close to the receiver for shallow events, and approaches some asymptotic value for events occurring at great depth. In the limiting case, as the offset/depth ratio approaches zero, the position of the conversion point asymptote is (Fromm et al., 1985):

$$x_p \approx \frac{\Delta x}{1 + \gamma} \ . \tag{6}$$

Although it is widely recognized that this formula is not accurate for shallow events (Slotboom and Stewart, 1989), it is nevertheless commonly used in the industry for CCP (CCP) trace sorting.

For a single elastic layer, the exact position of the conversion point can be obtained analytically. In their Appendix A, Tessmer and Behle (1988) show that the difference, D, between x_p and the source-receiver midpoint satisfies the fourth order polynomial equation:

$$D^4 + (z^2 - x^2/2)D^2 - z^2 k x D + 1/16(x^4 + 4x^2z^2) = 0 \ , \tag{7}$$

where z is the layer thickness, x is the source-receiver offset and $k = (1+\gamma^2)/(1-\gamma^2)$. Equations for the four solutions to (7) are given in Tessmer and Behle (1988, equation A10). In general, only two of the solutions are Real, and of these the correct solution satisfies the relation:

$$D \leq x/2 \ . \tag{8}$$

The solution to the exact single layer formula (7) can be utilized in two ways for P-SV processing. First, it is possible to selectively gather traces for optimum stacking for a single depth using this formula. In order to obtain an optimum image of multiple horizons, it is therefore necessary to regather and stack the data several times. An alternative to trace sorting is to reposition each sample point to its correct conversion point location, the "P-SV CCP map". This procedure can be cast in terms of a co-ordinate transformation:

$$\mathbf{u}(x_g,\Delta x,t) \xrightarrow{\text{Mapping Function}} \mathbf{u}'(x_p,\Delta x,t) \quad , \tag{9}$$

where x_g is the trace gather co-ordinate and $x_p(t)$ is the true conversion point co-ordinate. The mapping function utilized is calculated using the solution to (7), although ray tracing could also by employed. Because the data are discretely sampled it is necessary to interpolate $\mathbf{u}'$ after mapping. This procedure is more computationally intensive than a simple trace sort, but it provides optimum lateral resolution for all depth ranges and may be more efficient than regathering and stacking data several times.

Results

Both formulae for calculating the CCP position have been employed in a synthetic model study to compare the different methods of gathering and mapping P-SV converted wave data. For simplicity, a constant velocity background model was used, containing four mode conversion horizons (Figure 3). This earth model could be considered as a stack of constant velocity layers with varying densities. Each of the horizons has a 50 m step, analagous to a vertical normal fault. A synthetic field survey was generated using this model with geometrical parameters summarized in Table 1. Note that only mode converted reflections (not diffractions) were generated. These data were then processed using one of the following schemes:

Flow 1: Input → Sort (rebin) → NMO → Stack → Plot
Flow 2: Input → Sort → NMO → P-SV CCP map → Stack → Plot

Figure 4a shows a stacked section obtained using flow 1 and equation (6) for x_p. The step has not been accurately imaged at any depth, as is apparent from the overlap of events, although the magnitude of the approximation error decreases with depth. The apparent shorter event overlap on the shallowest event is an artifact of the NMO stretch mute. Figure 4b shows an example CCP gather at position 109, both before and after NMO corrections. Events that originated from

Table 1. Synthetic model acquisition parameters.

Number of channels	80
Spread type	End on
Source/receiver array type	single
Number of source points	17
Nominal fold coverage	10
Group interval	30 m
Source interval	120 m
Near offset	180 m
Far offset	2550 m

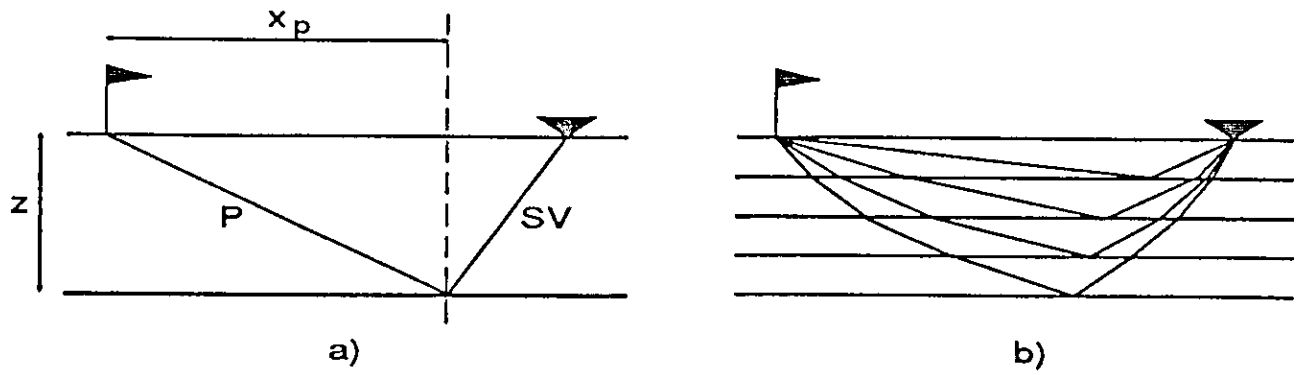

FIG. 2. (a) Raypath geometry for a P-SV converted reflection, single layer case. Note that the mode conversion point is shifted away from the midpoint toward the receiver. (b) Raypath geometry for P-SV converted reflections for the multilayer case. The conversion point position varies with depth.

both sides of the step are present in the same gather, thus resulting in some smearing of the stacked data. The dashed line on the uncorrected gather shows the mute profile used to process P-SV data from the Carrot Creek area (Harrison, 1989) having the same spread parameters.

Figure 5 depicts sections obtained using the exact formula for a single layer, and gathering depths of 250 m and 1000 m respectively. In Figure 5a, the position of the first step is accurately defined. The unusual appearance of the shallowest event is caused by alternating high and low stacking fold coupled with severe non-hyperbolic moveout. The position of the deeper steps are very poorly imaged. In contrast, the position of the deepest step in Figure 5b is accurately imaged, but the shallower events have become smeared. Lateral resolution can thus be selectively optimized for a specific depth by gathering traces using x_p calculated from the solution to equation (7). However, in order to achieve optimal resolution for multiple horizons, it is necessary to regather and stack the data.

Figure 6 shows the results obtained using the P-SV CCP map. In this case all four of the step positions have been accurately imaged. The slight degree of scatter in the data is probably caused by an excessively large bin dimension for offset. This problem can be overcome by utilizing a shorter group interval along with a greater number of channels, or by combining the P-SV CCP mapping process with stacking (Slotboom and Stewart, 1989). However, amplitude versus offset information is lost when the data are stacked. The current mapping algorithm has been implemented on the CREWES IBM 4381 computer, operating under the Western Geophysical IQUEUE™ processing system.

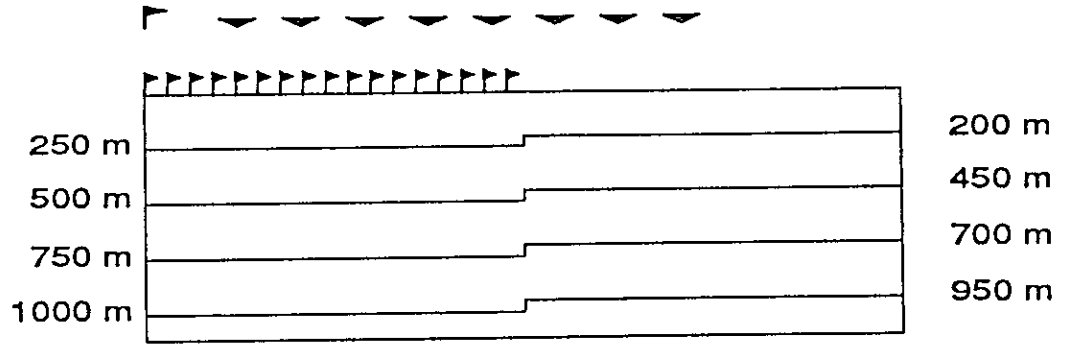

FIG. 3. Step function earth model used to generate synthetic data. Background velocities are α = 3000 m/s and β = 1500 m/s. Flags at the surface show positions of each source point. Above these, a source flag with every tenth receiver is shown to illustrate the spread dimensions relative to the model size.

Error analysis

With this new procedure, it is important to establish if the increased processing cost is justified by the improved resolution. One method of examining this is to consider the magnitude of the CCP position error introduced if equation (6) for x_p is used. Figure 7 shows a graph of CCP position error versus depth for a range of offsets, using a single layer with γ = 0.5. The graph also shows the first Fresnel radius for a P-SV converted reflection versus depth (see Appendix A). The intersection of the error curves with the Fresnel radius provides a guideline for the minimum depth for a given offset for which use of the asymptotic gather (equation 6) does not result in excessive smearing of the data. The intersection occurs at a depth of 800 m for an offset of 1500 m, and 1550 m for an offset of 2500 m, suggesting that current gathering methods are inadequate for P-SV events at long offsets.

If incorrectly gathered events are muted under normal circumstances, the additional effort involved with using the P-SV CCP map may be unjustified. Calculated mute profiles for various values of CCP smearing are shown in Figure 8. The same mute profile used in Figure 4b (Harrison, 1989) is also illustrated for comparison.

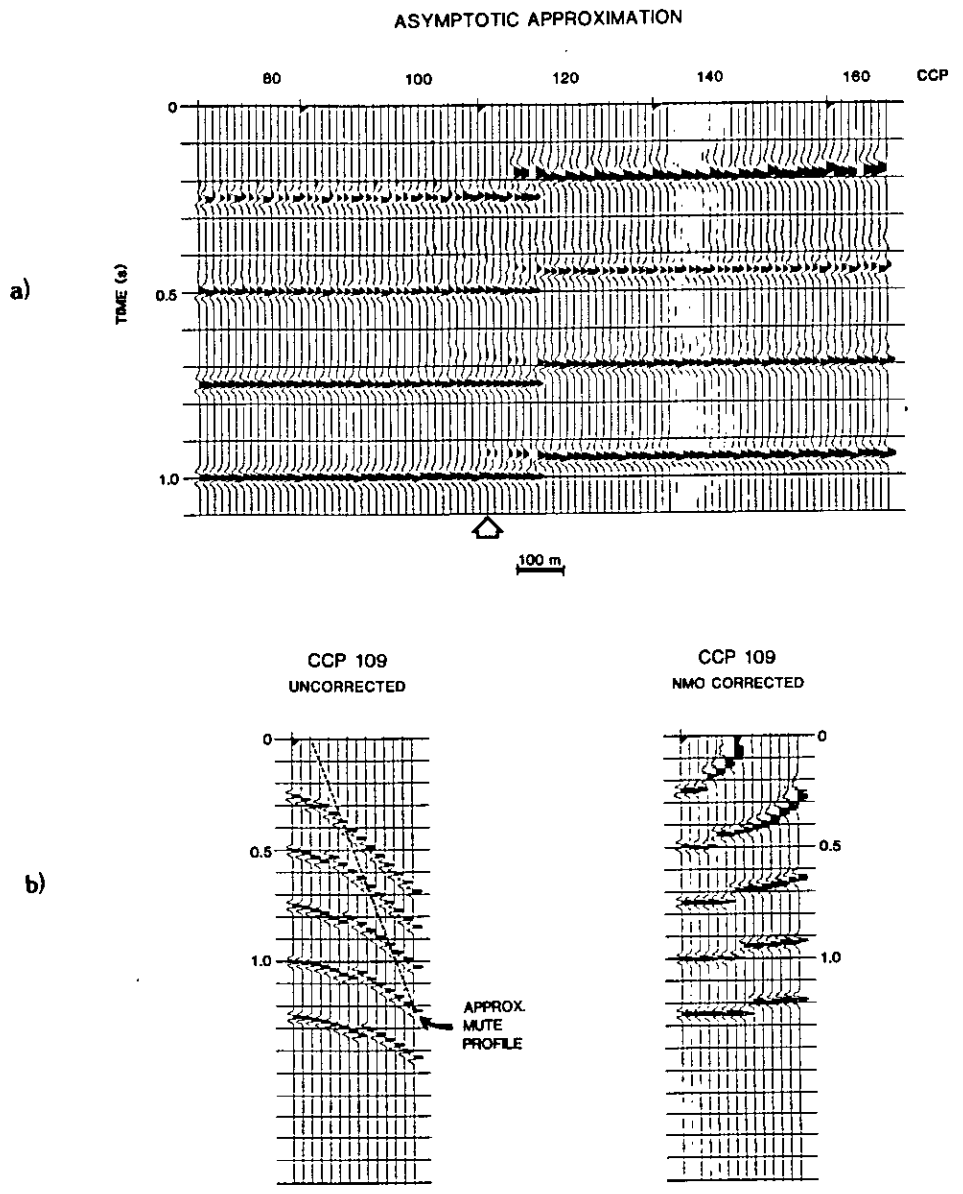

FIG. 4. (a) Stacked section from synthetic data over step model. Common conversion point gathering was performed using the asymptotic formula (equation 6). Note smearing of events due to incorrectly gathered data. Arrow shows position of CCP gathers in (b).
(b) Example CCP gather from position 109. The uncorrected gather on the left shows an example mute profile from the Carrot Creek area (Harrison, 1989), which was recorded using the same spread parameters. The NMO corrections for the gather shown on the right were applied using a velocity of $(\alpha\beta)^{1/2}$. The hyperbolic approximation is not valid at far offsets even for a single layer.

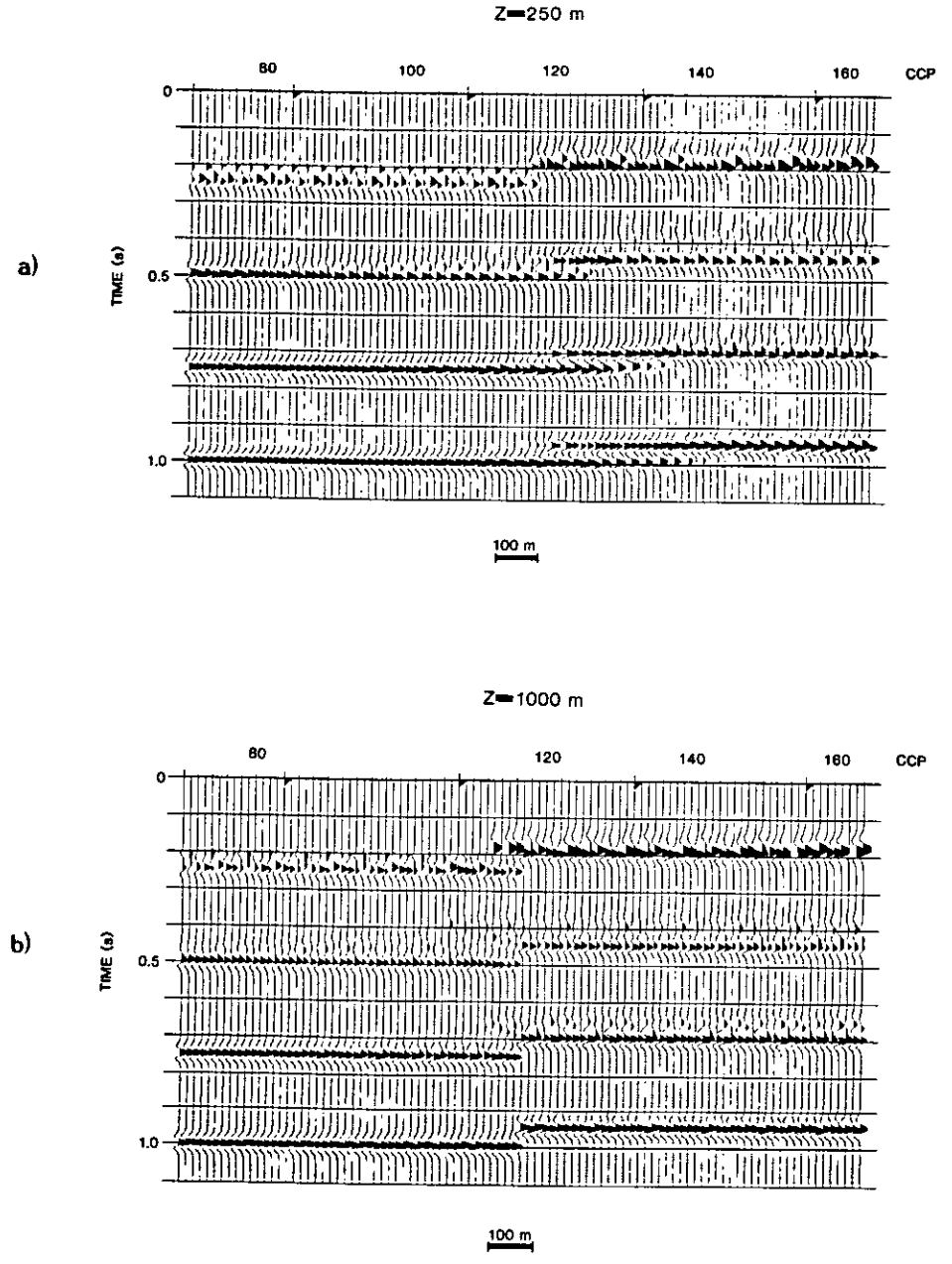

FIG. 5. (a) Stacked section from synthetic data over step model. Common conversion point gathering was performed using exact formula for a single layer (Tessmer and Behle, 1988) for a depth of 250 m. The position of the first step is accurately imaged; however deeper steps are badly smeared. Unusual appearance of the first event is caused by alternating high and low stacking fold. (b) Stacked section gathered using exact formula for a depth of 1000 m. The position of the deepest step has been accurately imaged.

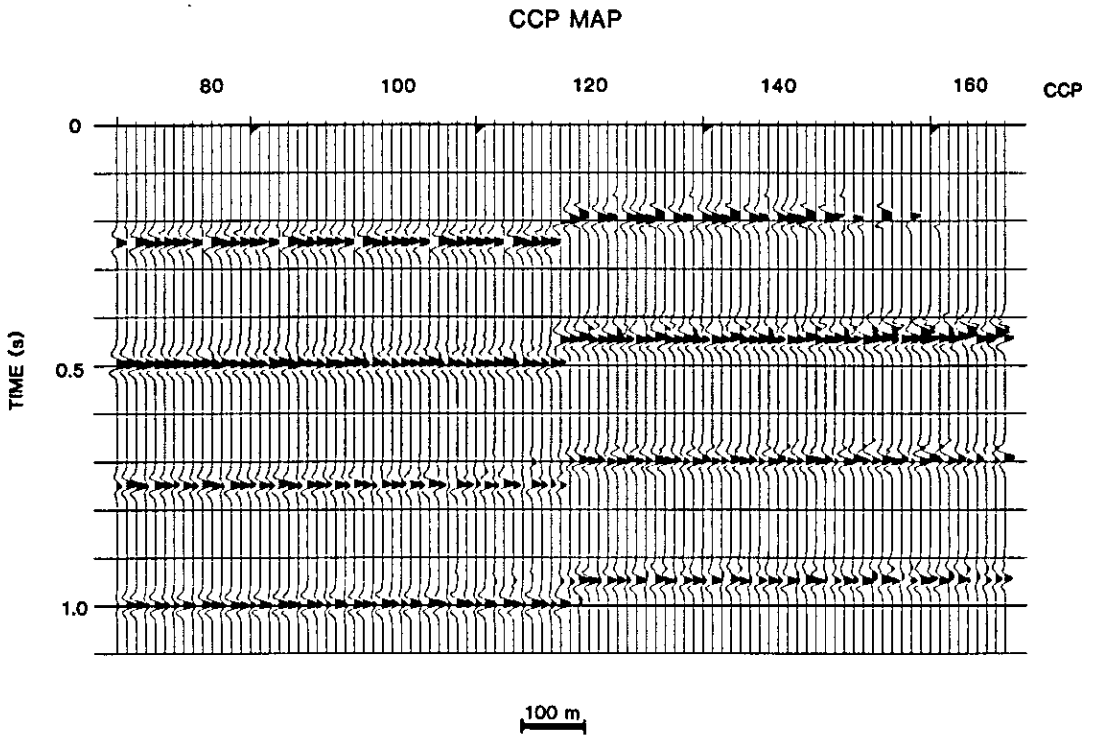

FIG. 6. Stacked section from step model synthetic data. P-SV CCP map was utilized rather than CCP gathering.

VELOCITY ANALYSIS

Tessmer and Behle (1988) demonstrated that the squared traveltime for a reflected P-SV wave is an even power series in x, as for the P-P case:

$$t_n^2 = c_1 + c_2x^2 + c_3x^4 + c_4x^6 + \ldots \quad , \tag{10}$$

and showed that the recursive formulae given by Taner and Koehler (1969) can be used to calculate the coefficients of the series. Formulae for the first three coefficients in the series are given in Appendix B. The first two coefficients are remarkable similar to the coefficients for the infinite series in the P-P case. The first coefficient, c_1, represents the squared two way vertical traveltime for the converted wave. The second coefficient in the series, c_2, represents the square of the reciprocal P-SV rms velocity ($1/\tilde{v}_{ps}^2$) (Tessmer and Behle, 1988). By truncating this power series after two terms, an approximate traveltime formula is obtained that is hyperbolic. However, this approximation is not as good as for the

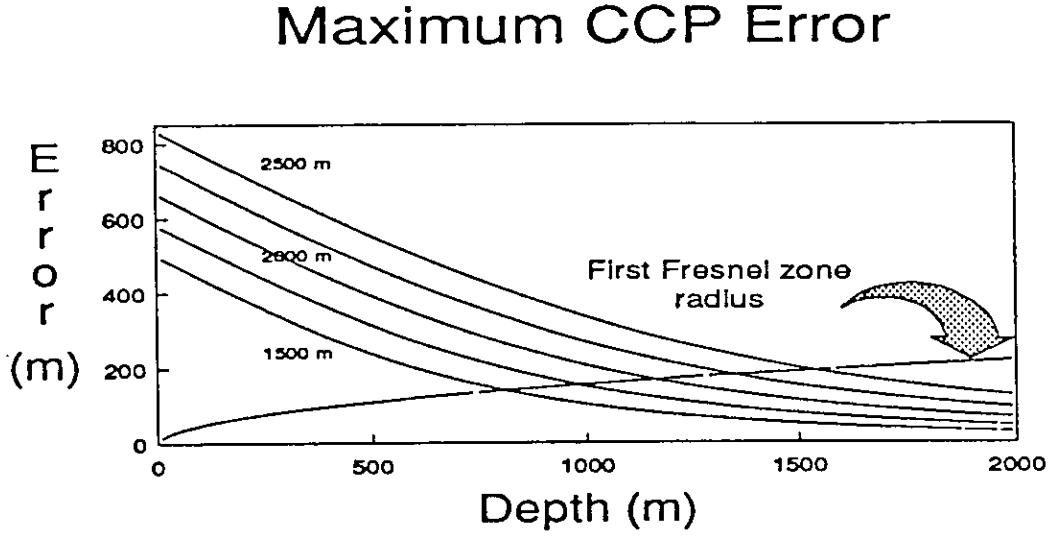

FIG. 7. Graph of error (ie. difference between asymptotic and exact conversion point formulae) vs. depth for various offsets between 1500 m and 2500 m. Also shown for comparison is the first Fresnel zone radius for P-SV converted reflections (see Appendix A).

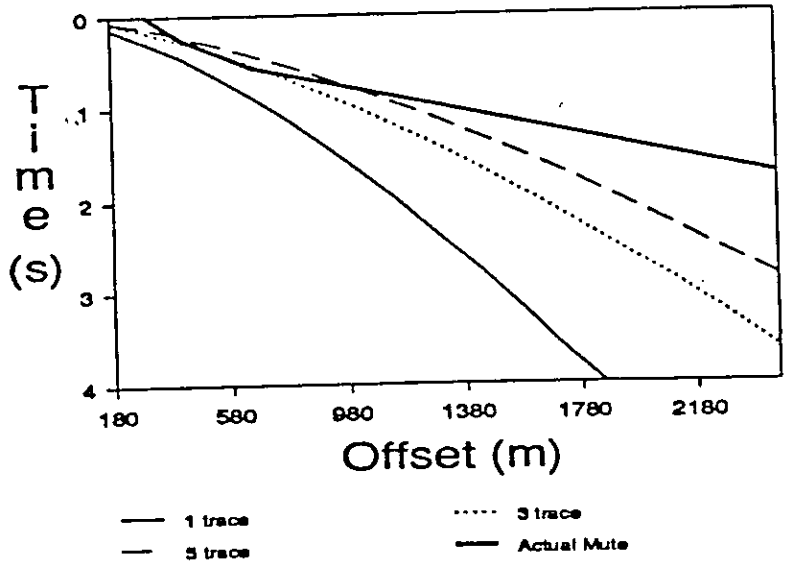

FIG. 8. Calculated CCP smear mute profile. A one trace mute excludes data with data smearing that exceeds one CCP interval, etc. Also shown is the actual mute profile applied to P-SV data from Carrot Creek (Harrison, 1989).

P-P case. For a single layer, the second coefficient reduces to:

$$c_2 = 1/(\alpha\beta) \tag{11}$$

Unlike the P-P case, however, the higher coefficients in the series do not become zero for a single layer. The third coefficient reduces to:

$$c_3 = \frac{2\alpha\beta - \alpha^3/\beta - \beta^3/\alpha}{4z^2(\alpha+\beta)^4} , \tag{12}$$

for the single layer case. Examination of the NMO corrected gather in Figure 4b demonstrates that the hyperbolic approximation is not accurate for shallow events at long offsets, even for the single layer case. These results suggest that some higher order approximation to the power series (11) may be necessary in general.

P-SV MIGRATION

Migration is a seismic imaging process that performs two related tasks; to reposition dipping reflectors into their true spatial position, and to collapse diffraction hyperbolae into single points. The study of seismic migration has become an important field in its own right, and many different algorithms have been developed for its implementation. Three techniques for performing migration based on the scalar wave equation have emerged: the Kirchhoff method, which is based on an integral solution to the wave equation and can be considered as an extension to the diffraction summation method, Stolt migration, which is performed in the *f-k* domain, and finite difference methods, which downward continue the wave field into the earth until the imaging condition (Claerbout, 1985) is achieved. However, because these methods are based on the scalar wave equation or a parabolic approximation to this equation, they fail to account for mode conversions and the presence of shear waves. Recent research has been directed toward the application of the elastic wave equation for prestack migration (eg. Kuo and Dai, 1984; Wapenaar, *et al*, 1987; Beydoun and Mendes, 1989). In addition to being extremely computationally demanding, however, these methods are highly sensitive to the estimate of γ in the velocity model (Etgen, 1988) in order to satisfy the *elastic* imaging condition (time and space coincidence of the P and SV wave fields).

In this study, the validity and inherent limitations of post-stack migration of separated P-SV data are investigated. Although similar in implementation, the procedure is conceptually less straightforward than the P-P case. For a simple layered earth model all events on a zero offset section have zero amplitude. Hence the amplitude of a scattered event after stack must be treated as the mean of the amplitudes over a range of offsets, but the traveltimes are considered as zero offset. For the layered earth case, the zero offset diffraction pattern from a point or line scatterer is symmetric and nearly hyperbolic. The same is be true for a P-SV section for constant γ. In the P-SV case for variable γ, the zero offset diffraction pattern resulting from a point scatterer becomes more complex.

P-SV scattering from an obstacle

In order to study the problem of post-stack P-SV migration, it is essential to fully understand the forward problem: the scattering of SV waves from an obstacle due to an incident P wave field. The geophysical scattering problem from barriers of arbitrary shape has been thoroughly addressed in the literature for the acoustic case (Trorey, 1970; Hilterman, 1970; 1975; Berryhill, 1980), using Kirchhoff's retarded potential method. A similar approach is possible using Kirchhoff-Helmholtz type integrals developed for the elastic wave equation by Pao and Varatharajulu (1976). It is more intuitive, however, to turn to the simplest possible geometry, for which analytical solutions for elastic wave scattering are available. The archetypal scattering problem in wave theory is scattering from a spherical obstacle. For a homogeneous, isotropic elastic space, the farfield displacement for a scattered SV wave from a rigid, infinitely dense sphere of radius a ($a << \lambda$) due to an incident plane P wave field is (Knopoff, 1959):

$$u_{sv} = \frac{-3\omega a\gamma^2 \sin\phi}{r\alpha(1+2\gamma^2)} e^{i\omega(t-r/\beta)} \qquad (13)$$

where ϕ is the angle subtended by the incident and scattered rays (Figure 9). The farfield displacement for the scattered P wave field is:

$$u_p = \frac{3\omega a \cos\phi}{r\alpha(1+2\gamma^2)} e^{i\omega(t-r/\alpha)} \qquad (14)$$

Two important observations can be made from equations (14) and (15):

Table 2. Synthetic model acquisition and processing parameters.

Number of channels	80
Spread type	split
Source/receiver array type	single
Number of source points	17
Nominal fold coverage	10
Group interval	20 m
Source interval	80 m
Near offset	120 m
Far offset	1700 m
Common conversion point gather	z=1000 m
NMO	$v=(\alpha\beta)^{1/2}$
Stack	
Finite difference migration	$v_m=2\alpha\beta/(\alpha+\beta)$

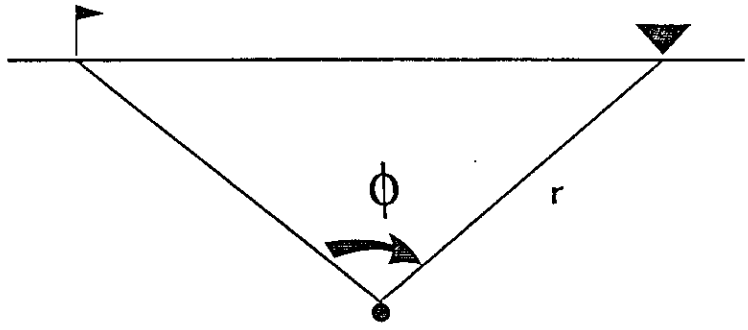

FIG. 9. P-SV scattering from a spherical obstacle.

•The scattered P wave field has a maximum amplitude for $\phi=0$ (ie. back toward the source), whereas the scattered SV wave field has a maximum amplitude for $\phi=\pi/2$.

•The maximum scattered SV wave displacement amplitude has a magnitude γ^2 greater than the maximum scattered P wave. This suggests that P-SV scattering from this type of obstacles on long offset recordings is at *least as significant* as P-P scattering.

Validity of the zero offset assumption

Even for P-P reflections, it is not intuitively obvious that the result of summing a series of velocity corrected traces sharing a common midpoint will result in a trace with amplitudes approximating a zero offset trace. It can be shown that for short offsets, the stacking velocity for a single diffractor in a homogeneous elastic medium is the P-wave velocity of the medium. This result assures the validity of the stacking process for short offsets, from a kinematic perspective. Berryhill (1978) showed that the amplitude versus offset relationship for scattering from an edge is largely governed by the distance of the CDP position from the edge, suggesting that the zero offset assumption for stacked P-P events is likely to be justified.

For P-SV reflections, the problem is more complex. Although the stacked amplitudes are not representative of the zero offset theoretical amplitudes for a point scatterer (zero for constant γ), the first order problem is to establish the kinematic validity of the stacking process. In Appendix C, it is shown that for short offsets, the stacking velocity of a point P-SV scatterer is $\tilde{v}_{ps}$. Coupled with the results of the previous section, we can expect to observe P-SV diffractions on a stacked section. Figure 10a shows a synthetic stacked section generated using equation (14) for five point scatterers embedded in a constant velocity medium with α = 3000 m/s and β = 1500 m/s. Acquisition and processing parameters are summarized in Table 2. The amplitudes of the stacked events is similar to the unstacked amplitudes, and the shape of the diffraction curves are nearly hyperbolic. Figure 10b shows the results of implicit 15° finite difference migration of the data in Figure 10a, using a migration velocity of (Appendix A):

$$v_m = 2\alpha\beta/(\alpha+\beta) \ . \qquad (16)$$

The migration has successfully collapsed all but the shallowest (z=250 m) point scatterers.

FUTURE WORK

Further algorithm testing is planned using both field data and data acquired using the CREWES physical modeling facility. Specific areas for future endeavour include:

- investigating means of determining the natural co-ordinate system (eg. by cross-correlation power spectra);
- formulation of a better method for calculating the P-SV CCP mapping function for layered media;
- Implementation of non-hyperbolic moveout for P-SV reflections.

SUMMARY

A number of aspects of P-SV seismic imaging have been considered, primarily from a theoretical perspective. It has been demonstrated that in areas having a low velocity near surface layer, S1-S2 wave field separation can be implemented by a simple co-ordinate rotation. The wave field separation should be performed prior to stack in order to correctly deal with the different stacking velocities of the fast and slow shear arrivals, and to improve data dependent processing steps such as automatic residual statics. A new method for CCP data rebinning has been proposed that provides superior lateral resolution when compared with the current practice of asymptotic CCP gathering. The characteristic moveout for P-SV converted events is nearly hyperbolic; however, hyperbolic moveout corrections are less accurate than for P-P events, and a higher order approximation to the true traveltime function may be necessary. finally, synthetic model studies suggest that migration of P-SV converted wave data may be possible with only slight modification to existing algorithms. These processes hold promise as an attractive alternative method to full elastic wave equation prestack migration as a method for accurate seismic imaging using P-SV reflections.

ACKNOWLEDGMENTS

I would like to thank Andre Latour of Western Geophysical and Tina Howell for their programming assistance.

REFERENCES

Aki, K. and Richards, P.G., 1980, Quantitative seismology: Theory and methods: Volume 1: W.H. Freeman & Co.

Alford, R.M., 1986, Shear data in the presence of azimuthal anisotropy: 56th Ann. Internat. Mtg., Soc. Expl. Geophys., Expanded Abstracts, 476-479.

Berryhill, J.R., 1977, Diffraction response for nonzero separation of source and receiver: Geophysics, 42, 1158-1176.

Beydoun, W.B. and Mendes, M., 1989, Elastic ray-Born l_2-migration/inversion: Geophys. J., 97, 151-160.

Chiburis, E.F., Kelamis, P.G. and Clement, W.G., 1988, Separation of P- and S-wave fields via

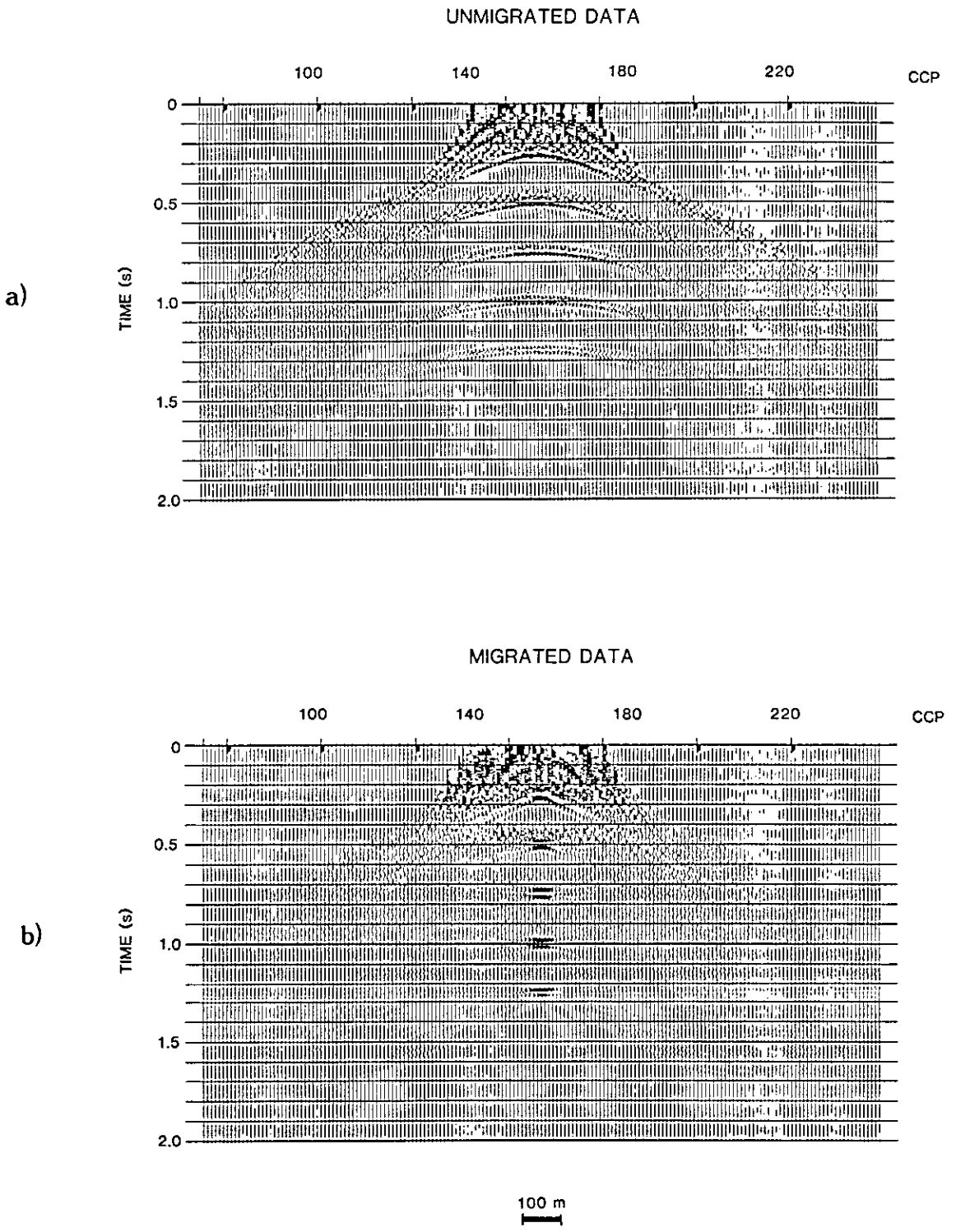

FIG. 10. (a) Stacked section for synthetic data generated using SV-wave scattering from five small spheres in a homogeneous elastic medium. (b) Results of finite difference time migration applied to data in (a).

the Tau-p transform: 58th Ann. Intern. Mtg., Soc. Expl. Geophys., Expanded Abstracts, 665-667.
Claerbout, J.F., 1985, Imaging the earth's interior: Blackwell Scientific Publications.
Crampin, S., 1981, A review of wave motion in anisotropic and cracked elastic-media: Wave motion, **3**, 343-391.
---------- 1985, Evaluation of anisotropy by shear-wave splitting: Geophysics, **50**, 142-152.
Dankbaar, J.W.M., 1985, Separation of P and S waves, Geophys. Prosp., **33**, 970-986.
Eaton, D.W.S., 1989, The free surface effect: Implications for amplitude-versus-offset inversion: J. Can. Soc. Expl. Geophys., in press.
Ensley, R.A., 1984, Comparison of P- and S-wave seismic data: A new method for detecting gas reservoirs: Geophysics, **49**, 1420-1431.
Etgen, J.T., 1988, Prestacked migration of P and SV waves: 58th Ann. Internat. Mtg., Soc. Expl. Geophys., Expanded Abstracts, 972-975.
Evans, R., 1984, Effects of the free surface on shear wavetrains: Geophys. J., **76**, 165-172.
Fromm, G., Krey, T. and Wiest, B., 1985, Static and dynamic corrections: *in* Dohr, G., Ed., Seismic shear waves: Handbook of Geophysical Exploration, Vol. 15a, Geophysical Press, 191-225.
Harrison, M., 1989, Carrot Creek 3 component data processing: this volume.
Hilterman, F.J., 1970, Three dimensional seismic modeling: Geophysics, **35**, 1020-1037.
---------- 1975, Amplitudes of seismic waves - a quick look: Geophysics, **40**, 745-762.
Knopoff, L., 1959, Scattering of compression waves by spherical obstacles: Geophysics, **24**, 30-39.
Kuo, J.T. and Dai, T., 1984, Kirchhoff elastic wave migration for the case of noncoincient source and receiver: Geophysics, **49**, 1223-1238.
McCormack, M.D. and Tatham, R.H., 1986, Shear-wave exploration seismology, course notes: SEG continuing education series.
Mora, P., 1987, Nonlinear two-dimensional elastic inversion of multioffset seismic data: Geophysics, **52**, 1211-1228.
Nuttli, O. and Whitmore, J.D., 1962, On the determination of the polarization angle of the S-wave: Bull., Seis. Soc. Am., **52**, 95-107.
Pao, Y.H. and Varatharajulu, V., 1976, Huygen's principle, radiation conditions and integral formulas for the scattering of elastic waves: J. Acoust. Soc.Am., **59**, 1361-1371.
Robertson, J.D. and Pritchett, W.C., 1985, Direct hydrocarbon detection using comparative P-wave and S-wave seismic sections: Geophysics, **50**, 383-393.
Slotboom, R.T. and Stewart, R.R., 1989: Depth-variant gathering of P-SV seismic data. Presented at the joint CSEG-CSPG convention.
Taner, M.T. and Koehler, F., 1969, Velocity spectra - digital computer derivation and applications of velocity functions: Geophysics, **34**, 859-881.
Tatham, R.H., 1982, V_p/V_s and lithology: Geophysics, **47**, 335-344.
Taylor, G., 1989, The point of P-S mode-converted reflection: An exact determination: Geophysics, **54**, 1060-1063.
Tessmer, G. and Behle, A., 1988, Common reflection point data-stacking technique for converted waves: Geophys. Prosp., **36**, 671-688.
Thomsen, L., 1988, Reflection seismology over azimuthally anisotropic media: Geophysics, **53**, 304-313.
Trorey, A.W. 1970, A simple theory for seismic diffractions: Geophysics, **35**, 762-784.
---------- 1977, Diffractions for arbitrary source-receiver locations: Geophysics, **42**, 1177-1182.
Wapenaar, C.P.A., Kinneging, N.A. and Berkhout, A.J., 1987, Principle of prestack migration based on the full elastic two-way wave equation: Geophysics, **52**, 151-173.
Willis, H.A., Rethford, G.L. and Bielanski, E., 1986, Azimuthal anisotropy: Occurence and effect on shear-wave data quality. Presented at the 56th Ann. Internat. Mtg., Soc. Expl. Geophys.
Yilmaz, O., 1987, Seismic data processing:, Investigations in Geophysics, Vol. 2, Soc. Expl. Geophys.

APPENDIX A

The two-way vertical traveltime for a P-SV converted event is (Figure A-1):

$$t = z(1/\alpha+1/\beta) = z\ \frac{\alpha+\beta}{\alpha\beta} \tag{A-1}$$

The two-way traveltime for the non-vertical raypath is:

$$t' = (z^2+r^2)^{1/2}(1/\alpha+1/\beta) = (z^2+r^2)^{1/2}\ \frac{\alpha+\beta}{\alpha\beta} \tag{A-2}$$

In order for the events to summ constructively, the traveltime difference must satisfy:

$$t'-t = \frac{\alpha+\beta}{\alpha\beta}[(z^2+r^2)^{1/2}-z] \le T/2 \tag{A-3}$$

where T is the dominant period. Hence,

$$(z^2+r^2)^{1/2} \le \frac{\alpha\beta}{\alpha+\beta}\bullet\frac{T}{2} + z \tag{A-4}$$

The migration velocity for a constant velocity medium is:

$$v_m = \frac{2\alpha\beta}{\alpha+\beta} \tag{A-5}$$

And using the relation $T = 1/f$, where f is the dominant frequency, A-4 can be rewritten:

$$(z^2+r^2)^{1/2} \le v_m/4f + z \tag{A-6}$$

Squaring both sides gives:

$$z^2 + r^2 \le v_m^2/16f^2 + v_m z/2f + z^2 \tag{A-7}$$

so that:

$$r \le (v_m^2/16f^2 + v_m z/2f)^{1/2} \tag{A-8}$$

If $z >> v_m/f$, we can write:

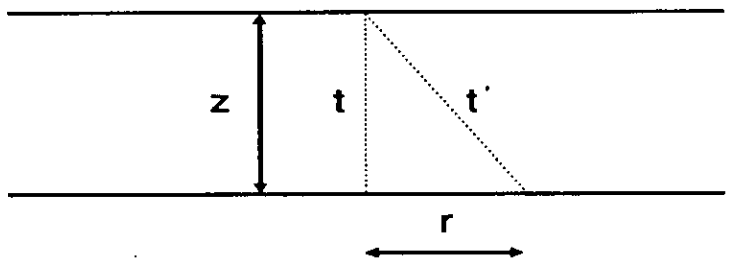

FIG. A-1: Fresnel radius calculation for converted waves.

$$r \leq (v_m z/2f)^{1/2} \tag{A-9}$$

Therefore the Fresnel radius for P-SV converted waves is $(v_m z/2f)^{1/2}$. Note that the P-wave Fresnel zone is given by:

$$x_p^2 = z\alpha/2f \tag{A-10}$$

If, for example, we consider the case where $\gamma=1/2$, then $x_{ps}^2 = z\alpha/3f$. Thus we see that the converted-wave Fresnel zone radius is smaller that the P-wave Fresnel zone radius. This result suggests that the lateral resolution of unmigrated P-SV data is somewhat better than that for the corresponding P-P data.

APPENDIX B

Tessmer and Behle (1988) showed that the squared traveltime for P-SV converted reflections for a horizontally layered earth can be expressed as an even power series:

$$t^2 = c_1 + c_2x^2 + c_3x^4 + \ldots \tag{B-1}$$

The coefficients in this power series can be determined for the nth layer using the formulae of Taner and Koehler (1969). The first three coefficients are given by:

$$\begin{aligned} c_1 &= a_1^2 \\ c_2 &= a_1/a_2 \\ c_3 &= a_2^2 - a_1a_3/4a_2^4 \end{aligned} \tag{B-2}$$

where:

$$a_m = \sum_{k=1}^{n} h_k(\alpha_k^{2m-3}+\beta_k^{2m-3}) \tag{B-3}$$

Using (B-3), we can expand (B-2):

$$c_1 = \{ \sum_{k=1}^{n} h_k(1/\alpha_k+1/\beta_k) \}^2 = t_0^2 \tag{B-4}$$

$$c_2 = \frac{\sum_{k=1}^{n} h_k(1/\alpha_k+1/\beta_k)}{\sum_{k=1}^{n} h_k(\alpha_k+\beta_k)} = 1/\tilde{v}_{ps}^2 \tag{B-5}$$

$$c_3 = \frac{\{ \sum_{k=1}^{n} h_k(\alpha_k+\beta_k) \}^2 - \sum_{k=1}^{n} h_k(1/\alpha_k+1/\beta_k) \cdot \sum_{k=1}^{n} h_k(\alpha_k^3+\beta_k^3)}{4\{ \sum_{k=1}^{n} h_k(\alpha_k+\beta_k) \}^4} \tag{B-6}$$

where t_0 is the vertical two-way traveltime and $\tilde{v}_{ps}$ is the P-SV rms velocity.

APPENDIX C

Consider the raypath geometry shown in Figure C-1. It will be shown that the stacking velocity at short offset x for the diffracted event is $\sqrt{\alpha\beta}$ (ie. the correct stacking velocity for a horizontal reflector). If the lateral distance from the source to the conversion point is x_1, from the conversion point to the receiver is x_2 and the depth to the scatterer (taken to be infinitesimal) is h then the traveltime equation is:

$$t = \frac{[h^2 + (X-x_1)^2]^{1/2}}{\alpha} + \frac{[h^2 + (X+x_2)^2]^{1/2}}{\beta} \qquad \text{(C-1)}$$

Expanding this expression gives:

$$t = \frac{[h^2 + X^2 + x_1^2 - 2Xx_1]^{1/2}}{\alpha} + \frac{[h^2 + X^2 + x_2^2 + 2Xx_2]^{1/2}}{\beta} \qquad \text{(C-2)}$$

Dropping higher order terms in the binomial expansion of C-2 gives:

$$t \approx \frac{[h^2 + X^2]^{1/2}}{\alpha} + \frac{[h^2 + X^2]^{1/2}}{\beta} + \frac{[x_1^2/\alpha + x_2^2/\beta]}{2(h^2 + X^2)^{1/2}} + \frac{X\,[x_2/\beta - x_1/\alpha]}{(h^2 + X^2)^{1/2}} \qquad \text{(C-3)}$$

assuming that $h^2 + X^2 >> x_1^2 - 2Xx_1$ and $h^2 + X^2 >> x_2^2 + 2Xx_2$. This implies that the source-receiver offset x is small relative to the depth to the scatterer. If we further assume that x_1 is related to x by the relation $x_1 = \Delta x/(1+\gamma)$ (equation 6) then the last term in A-3 can be dropped. Letting the traveltime for $x_1 = x_2 = 0$ be denoted t_0 we can now write the traveltime equation as:

$$t \approx t_0 + \frac{[x_1^2/\alpha + x_2^2/\beta]}{2(h^2 + X^2)^{1/2}} \qquad \text{(C-4)}$$

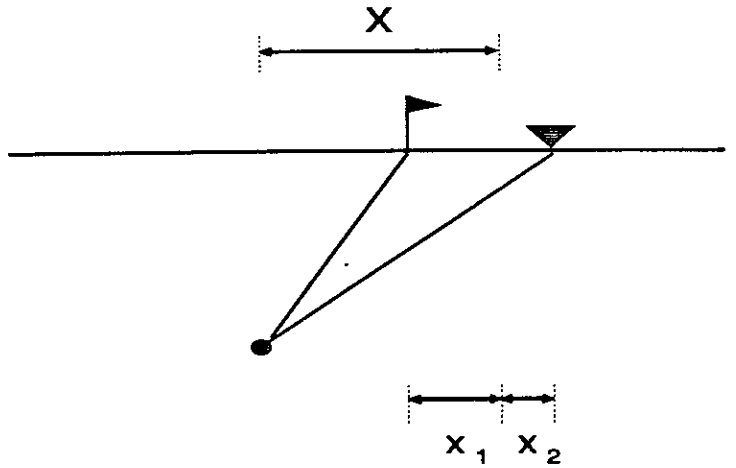

FIG. C-1. Two-way traveltime from a point scatterer.

Substituting for x_1 and x_2 gives:

$$t \approx t_0 + \frac{\Delta x^2}{2(h^2 + X^2)^{1/2}} \cdot \frac{\beta(1 + 1/\gamma)^2 + \alpha(1 + \gamma)^2}{\alpha\beta(1 + \gamma)^2(1 + 1/\gamma)^2} \qquad \text{(C-5)}$$

Squaring both sides of C-5 and again invoking the Binomial Theorem, assuming that the second term in C-5 is $<< t_0$ gives:

$$t^2 \approx t_0^2 + \frac{x^2}{(h^2 + X^2)^{1/2}} \cdot \frac{\beta(1 + 1/\gamma)^2 + \alpha(1 + \gamma)^2}{\alpha\beta(1 + \gamma)^2(1 + 1/\gamma)^2} \cdot$$

$$(h^2 + X^2)^{1/2}(1/\alpha + 1/\beta) \qquad \text{(C-6)}$$

recalling that $t_0 = (h^2 + X^2)^{1/2}(1/\alpha + 1/\beta)$. It is easily confirmed that C-6 simplifies to:

$$t^2 = t_0^2 + x^2/\alpha\beta \qquad \text{(C-7)}$$

Hence the traveltime equation for P-SV scattering from a point simplifies for short offsets to the NMO equation for P-SV reflections from the base of a single layer (Tessmer and Behle, 1988), confirming the *kinematic* validity of the CCP stacking process for P-SV diffractions.